

## W7-AS; Programme and Recent Results

KICK Manfred\*, WAGNER Friedrich and the W7-AS Team  
Max-Planck-Institut für Plasmaphysik, EURATOM Ass.  
D-85748 Garching, Germany

(Received: 30 September 1997/Accepted: 22 October 1997)

### Abstract

The programme of W7-AS concentrates mainly on topics related to the optimisation principles of the WENDELSTEIN stellarator line such as improved equilibria with reduced Shafranov shift, neo-classical transport in improved magnetic configurations including the effects of the ambipolar radial electric field, confinement of high energetic particles, radial diffusion of trapped electrons generated by ECR power deposition. But also topics related to stellarator physics, more generally, are intensely treated, such as the radiative limit at high densities, particle transport, GAE-modes, fluctuations and turbulence, the influence of shear on confinement, and the H-mode. Furthermore new diagnostics with respect to long pulse operation of W7-X are developed. Optimum (neoclassical) confinement discharges with energy confinement times (up to 50 ms) of more than 2.5 times larger than predicted by the International Stellarator Scaling, ISS95, with  $T_i \leq 1.5$  keV are presented as well as discharges with  $T_e \approx 4$  keV showing a strongly positive ECRH driven "electron root" feature of the radial electric field and high density high power NBI discharges leading to  $\langle \beta \rangle = 1.8\%$ . A 3D Edge code is developed to model edge transport and to optimise energy and particle deposition in a future island divertor. The role of  $E \times B$  drifts in islands is considered in detail. Heating scenarios with relevance to W7-X are finally addressed which are independent of cut-off densities and do not necessarily require magnetic resonance conditions, such as the O-X-B heating scenario of ECR waves. The prospects of ICRH for long pulse operation are explored.

### Keywords

W7-AS, stellarator, optimum confinement, transport, ISS95, electric field, ion root, electron root, equilibrium, heating scenarios

### 1. W7-AS

WENDELSTEIN 7-AS, W7-AS, is an Advanced Stellarator [1] (torus radius 2 m, effective plasma radius  $\leq 0.18$  m) with 5 toroidal periods. The magnetic configuration, with  $B_0 = 2.5$  T in the standard case, is optimised by a reduction of the Pfirsch-Schlüter currents. It is generated by a system of 9 non-planar coils in each period with 10 additional planar coils allowing a variation of the rotational transform,  $\iota$ , from 0.25 to 0.6. It has low shear and stability is given by a moderate magnetic well [2]. Different heating scenarios, electron cyclotron resonance heating, ECRH, with  $P \leq 0.4$

MW at 70 GHz and  $P \leq 1.2$  MW at 140 GHz, ion cyclotron resonance heating, ICRH, with  $P \leq 0.5$  MW at the antenna as well as neutral beam injection, NBI, ( $P \leq 3.5$  MW, 50 keV) give access to net current free plasmas in a wide range: electron densities,  $n_e \leq 3 \times 10^{20}$  m<sup>-3</sup> [3], electron temperatures,  $T_e \leq 4$  keV [4-6], ion temperatures,  $T_i \leq 1.5$  keV [7-9], and energy confinement times,  $\tau_E \leq 50$  ms [10]. All above results have been derived with a magnetic field on axis of  $B_0 \leq 2.5$  T.  $\langle \beta \rangle \leq 1.8\%$  has been achieved at  $B_0 \leq 1.25$  T (see chapter 3.3). The theoretically predicted reduction of

\*Corresponding author's e-mail: kick@ipp.mpg.de

the Shafranov shift by a factor of 2 has been proven experimentally already in an early stage of operation [3]. The bootstrap current of several kA can be compensated integrally either by a small ohmic current or more locally by current drive by ECR [11]. Current drive also can be used to introduce shear for better confinement [4,12]. With 0.4 MW ECRH at 140 GHz at high densities H-mode transitions with the characteristics as known from tokamaks could be achieved [13].

Plasma build-up can be carried out not only by ECRH but also by non-resonant Rf at 900 MHz leading to a low density target for NBI thus allowing operation independently of the "electron cyclotron resonance fields" of 2.5 and 1.25 T, respectively. Also independent on resonant magnetic fields is the O-X-B heating scenario [14,15] which recently has been successfully applied at W7-AS. ICRH has been operated successfully with long pulses of up to 1s [16].

## 2. Programme

The major element of the optimisation is to reduce the relative Pfirsch-Schlüter current  $\langle j_{\parallel}^2/j_{\perp}^2 \rangle$  and for W7-X to reduce the bootstrap current. Low PS currents lead to improved equilibria with small Shafranov shift, high stability and strongly reduced neoclassical losses; the minimisation of the bootstrap current avoids a strong disparity between high pressure vacuum field equilibria so that the characteristics of the field design are maintained towards high beta. The optimisation rests on the reduction of average curvature by proper plasma shaping, the repulsion of trapped particles from zones of high curvature by the mirror effect and from a proper match of toroidal and helical curvature. Despite of the optimisation neoclassical transport displays the deleterious  $1/\nu$  collisionality scaling in the long mean free pass, *lmfp*, regime. The presence of an ambipolar field will further reduce the transport coefficients to a tolerable level. It is mandatory to measure the ambipolar field and to assess the balance of radial species flow. If the ambipolar electric field is determined by radial neoclassical fluxes — because the superimposed turbulent contributions are low or intrinsically ambipolar — various transport equilibria (roots) might develop. Both negative and positive electric fields reduce the neoclassical ion losses. The electron root which develops at high electron temperature with thermally decoupled ions has the advantage of good electron and low impurity confinement. Stellarator optimisation is expected to improve also the confinement of energetic particles (in case of a reactor that of the  $\alpha$ -particles).

W7-AS is partly optimised in its field properties and can therefore address some of the above issues. The improvement in equilibrium is well documented [3,8]; the maximal beta is in the range  $\langle \beta \rangle \approx 1.8\%$  and is well above that of a classical stellarator [3,9]. The bootstrap current is dominated by toroidal curvature in W7-AS and increases the rotational transform just like in a tokamak. The measured bootstrap current agrees with the expected one in a large range of collisionalities [11].

The ambipolar electric field and its impact on transport will be discussed in detail below.

The confinement of NBI ions is complete in case of slowing down times  $\tau_s$  smaller than the energy confinement time  $\tau_E$ . For cases with high  $T_e$  when  $\tau_s$  can be much larger than the thermal  $\tau_E$ , the measured slowing down spectra cannot be modelled satisfactorily with the assumption of complete ion confinement. The discrepancy between measurement and the expectation from good confinement is also borne out by neutron flux measurements in case of D into D-injection. The results are still preliminary and the loss mechanisms are not yet identified [17]. With respect to transport of energetic electrons the fast radial diffusion of trapped electrons, heated by the interaction with ECRH, is observed in power deposition measurements (fast ECRH modulation). The deposition profile deviates from that expected from ray-tracing and absorption and shows wings in the plasma periphery [18]. The widening of the deposition profile is well modelled [19].

There are important topics in the development of stellarators which are, at present, beyond the reach of a rigorous optimisation like the high density operational range [20], turbulent transport [21,22], aspects of MHD stability like the beam induced Global Alfvén waves, GAE, [22,23], and the exhaust conditions. Present stellarators can operate at high density (see chapter 1) which will ease the conditions for plasma exhaust. In addition, stellarators can safely operate at high density. The operational limit is not connected with a virulent MHD phenomenon but is a radiative loss of plasma energy. Therefore, the collapse time is slow along the energy confinement time, the plasma energy is homogeneously distributed by radiation and there is time to interfere and to restore a stable plasma [20]. The confinement of W7-AS is determined by the superposition of neoclassical transport in the plasma core and turbulent transport in the gradient region towards the edge. The global confinement is determined by the turbulent processes. The pattern of confinement of the low-shear field system of W7-AS is rather capricious. Depending

on the choice of rotational transform  $t$  confinement can be good or low. The energy content  $W$  shows a strong variability with  $t$ . The following picture emerges: The confinement is good, when the iota profile fits into a iota range (edge to core) with few low-order resonances as it is the case around the major resonances  $1/3$  and  $1/2$ . Outside these intervals, shear is required for good confinement [4,12]. Sufficient shear is provided by PS- and bootstrap-current — if the plasma beta is large enough. Outside the resonances free intervals, the development of good confinement depends on a cyclic process because improved confinement enhances the pressure-driven currents which feedback positively on confinement. If the pressure driven currents are enforced by operation at high beta or low collisionality, the interplay between pressure driven currents and confinement is avoided and the sensitivity of  $W$  on  $t$  is lost. Because of the complexity of the dependence of energy content and field distribution not yet all details are satisfactorily understood.

The base-line confinement of W7-AS is provided in the good confinement intervals. It resembles the L-mode confinement of tokamaks. In these  $t$ -ranges and possibly with further restrictions, improved confinement regimes can develop. It is important that the conditions of external confinement as provided in stellarators are also capable of allowing states with improved confinement. An example which is well summarised in the literature is the H-mode of W7-AS [13]. Below, another regime is described.

### 3. Recent Results

Selected topics from the W7-AS programme are briefly discussed below.

#### 3.1 Optimum confinement discharges

At W7-AS, purely NBI heated and combined NBI/ECRH discharges at medium and high electron densities,  $n_e$  between  $1.1 \times 10^{20}$  and  $0.5 \times 10^{20} \text{ m}^{-3}$ , with  $T_e \geq T_i \approx 0.8\text{--}1.5 \text{ keV}$  lead to high performance if good wall conditioning and low recycling are provided. Energy confinement times up to  $\tau_E = 50 \text{ ms}$  are determined. The experimental transport analyses in the plasma core are consistent with the neoclassical predictions from DKES code [24,25].

In purely NBI heated discharges with a power of  $P_{\text{NBI}} \leq 400 \text{ kW}$ ,  $\tau_E \approx 50 \text{ ms}$  has been determined [10], exceeding the *ISS95* scaling [26] by more than a factor of 2.5, see Fig. 1. During the gradual transition to good confinement the density profile becomes narrower, whereas the temperature profile broadens. In both

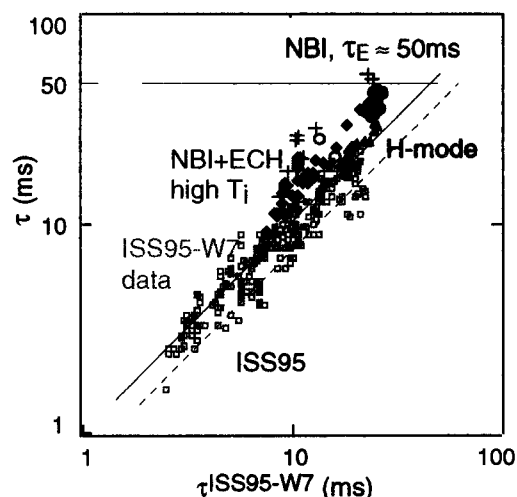


Fig. 1 Energy confinement times in W7-AS compared to *ISS95*-W7. Dashed line: *ISS95* for all helical devices; solid line: *ISS95*-W7 for W7-AS data up to 1995; open squares: pure ECRH; full triangles: ECRH H-mode; full circles: low power NBI, leading to  $\tau_E \approx 50 \text{ ms}$ , open circles: NBI with higher power; full (light) diamonds: combined NBI and ECRH, leading to  $T_i \approx 1.5 \text{ keV}$ . Crosses for the same discharges taking the kinetic energy instead of the diamagnetic one. Both, circles and diamonds, show the increase of  $\tau_E$  by about a factor of 2.5 compared to *ISS95*.

profiles the gradients steepen and the radial electric field  $E_r$  decreases in the gradient region to  $E_r \leq -300 \text{ V/cm}$  [10]. Both, density and temperature show very low values at the edge. Also in high power combined NBI/ECRH discharges, narrow density profiles, steep temperature gradients and large negative  $E_r$  (up to  $-700 \text{ V/cm}$ ) close to the plasma edge are found where locally  $n_e$  becomes very small (Fig. 2). For this type of discharges with  $T_e > T_i \leq 1.5 \text{ keV}$ , optimum confinement properties are found.  $\tau_E$  exceeds the *ISS95* scaling by a factor of about 2.5 as in the purely NBI heated case (Fig. 1). The experimental particle fluxes as well as the ion and electron energy fluxes are in good agreement with the neoclassical predictions up to  $r_{\text{eff}} = 12 \text{ cm}$ , see Refs. [7-9]. The radial electric field,  $E_r$ , obtained from the ambipolarity condition of the neoclassical fluxes is consistent with the experimental one deduced from the poloidal rotation of tracers measured by active CXRS in the plasma core (up to 12 cm) as well as by electron impact spectroscopy [27] and probe measurements [28] at the edge. The observation of neoclassical ambipolar radial electric fields up to the very edge where the turbulent fluxes dominate the neoclassical ones indicate that the *anomalous* particle fluxes are intrinsically ambipolar. Deviations in the intermediate range may be

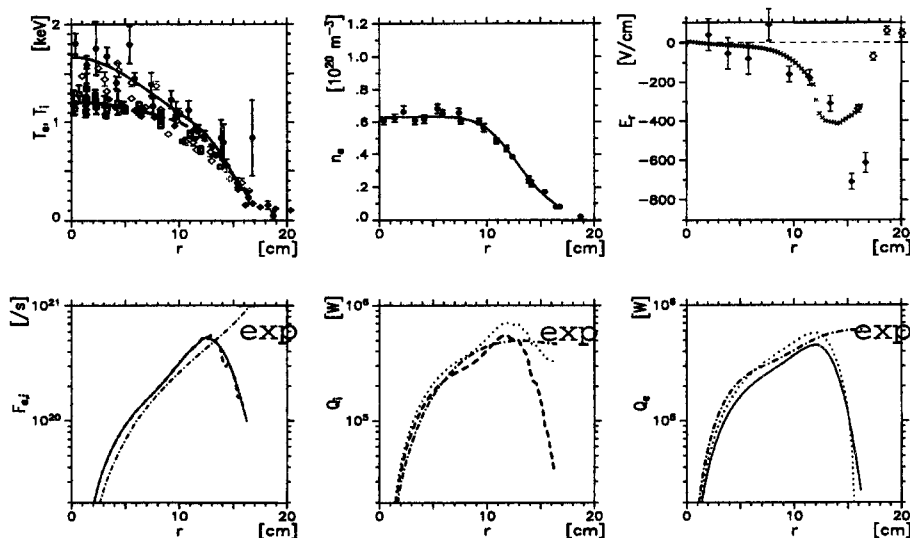


Fig. 2 Optimum confinement. Discharge #34313, combined ECRH and NBI,  $P_{\text{ECRH}} \approx 750$  kW,  $P_{\text{NBI}}^{\text{abs}} \approx 900$  kW, at medium density.  $T_e$  from Thomson scattering and ECE (dark symbols) and  $T_i$  (light symbols) from active CX-NPA and CXRS (upper left);  $n_e$  from Thomson scattering (upper middle), radial electric field (upper right) as deduced from active CXRS, (dots) and passive spectroscopy (circles) compared to the neoclassically calculated ambipolar electric field (crosses). In the lower part the experimental particle and energy fluxes for ions and electrons, respectively, are compared with neoclassical predictions by DKES code taking the ambipolar electric field (upper right) into account.

due to the violation of the condition of small electric fields for neoclassical theory [18].

In all discharges with optimum confinement the measured density profiles at outer radii are very similar for all central densities from  $0.5$  to  $1.1 \times 10^{20} \text{ m}^{-3}$  and heating powers between  $0.4$  and  $1.3$  MW. Also, the  $T_e$  and  $T_i$  profiles are very similar in this region [18]. Prerequisites for this type of discharges are good wall conditioning and very low recycling in order to obtain narrow density profiles and to provide global density control even for high NBI power levels with the related strong particle sources of up to  $2.5 \times 10^{20} \text{ s}^{-1}$ . All discharges have been carried out at  $t \approx 1/3$  at  $B_0 = 2.5$  T with a vertical field,  $B_z \approx 0.01 \times B_0$ . As a consequence the plasma is shifted towards the inboard limiters thus influencing the recycling behaviour but also the magnetic configuration is improved with respect to neoclassical transport, because the magnetic ripple at the location of strong (grad B) is reduced [29]. Once the above described conditions are fulfilled optimum confinement is reproducibly attained. During the next experimental campaign the question of attaining optimum confinement under separatrix conditions around  $t \approx 1/2$  will be a major topic of investigation.

### 3.2 ECRH driven "electron root" feature

In low density discharges, heated by ECR ( $P_{\text{ECRH}} = 400$  kW, 2nd harmonic X-mode at 140 GHz), very

strong positive  $E_r$  of up to  $+600$  V/cm close to the plasma centre with peaked electron temperature profiles and  $T_e(0) \approx 4$  keV,  $T_i(0) \approx 0.3$  keV and flat density profiles ( $n_e(0) \approx 0.2 \times 10^{20} \text{ m}^{-3}$ ) have been measured [4-6], see Fig. 3.  $\chi_e$  in the intermediate radial range agrees with the neoclassical prediction for the slightly positive  $E_r$  (ion root), in the centre it is larger than calculated for the neoclassical (thermal) electron root but much lower than neoclassically predicted if  $E_r$  is assumed to be zero, see Fig. 3. These large positive electric fields, correlated with strongly peaked electron temperature profiles have only been found at X-mode ECRH with powers above 400 kW in magnetic configurations of W7-AS where a significant part of the ECRH power is absorbed by ripple trapped electrons close to the axis [4-6,18]. These features are lost if the ECRH power is decreased or if the configuration is changed such that the toroidal ripple is reduced. The evidence, that ripple-trapped suprathermal electrons induced by ECRH generate the strong positive  $E_r$  in the centre, is supported by Monte Carlo simulations (in 5D phase space) [19].

### 3.3 Equilibrium and stability

For a discharge heated by about 2.2 MW of NBI at  $B_0 = 1.25$  T with  $B_z = 0.026 \times B_0$  with  $n_e(0) = 2 \times 10^{20} \text{ m}^{-3}$  and  $T_i \approx T_e = 0.35$  keV the free boundary equilibrium code NEMEC [30] predicts a central  $\beta_0$  of 4%

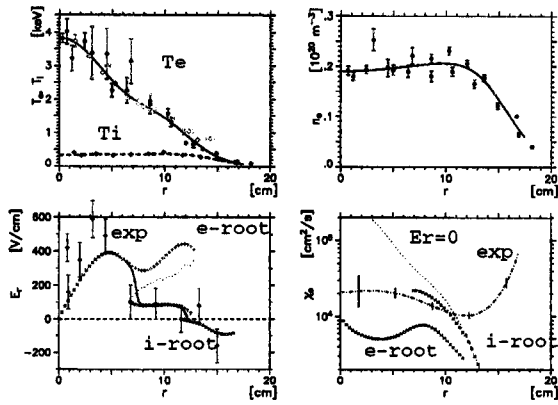


Fig. 3 "Electron root" feature. Low density ECR heated,  $P_{\text{ECRH}} \approx 750$  kW, discharge with strongly peaked  $T_e$  (upper left). The strongly positive electric field from CXRS is compared to the neoclassical electron root close to the centre and slightly positive ion root at intermediate radii (lower left). The lower right picture shows the experimental heat conductivity (dash-dotted line) compared to neoclassical predictions if  $E_r = 0$  is assumed (dotted line) and if electron and ion roots of  $E_r$  are taken into account (crosses).

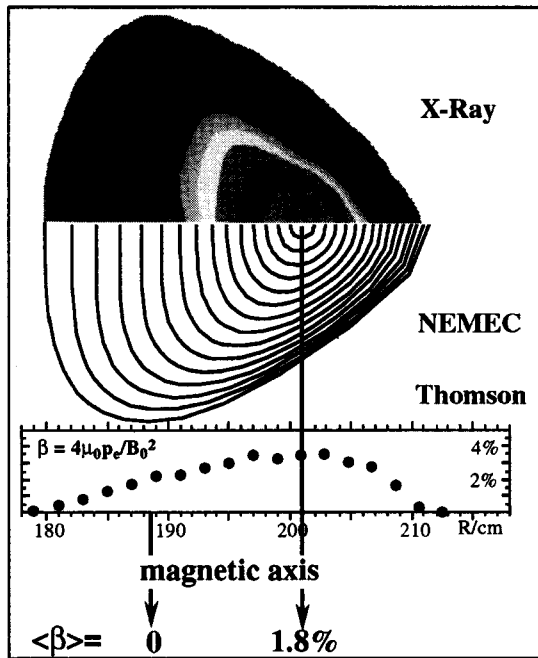


Fig. 4 Tomographic reconstruction of soft X-ray emission compared to magnetic flux surfaces calculated by NEMEC code for high  $\beta$  discharge heated by about 2.2 MW of NBI at  $B_0 = 1.25$  T with  $B_z = 0.026 B_0$ ,  $n_e(0) = 2 \times 10^{20} \text{ m}^{-3}$  and  $T_i \approx T_e = 0.35$  keV. The shift of the magnetic axis agrees well with that resulting from the  $\beta$  profile calculated from Thomson scattering.

and an averaged  $\langle \beta \rangle$  of 1.8%. This is in excellent agreement with the  $\beta$  profile evaluation from Thomson scattering data, see Fig. 4, where the ion contribution is estimated neglecting the effect of  $Z_{\text{eff}}$  which is expected to be small for this discharge. Furthermore the shift of the magnetic axis as deduced from the maximum of the  $\beta$  profile agrees very well with the NEMEC code result. Though the Shafranov shift of W7-AS is reduced by a factor of 2 compared to classical stellarators [3] it is still considerable. Nevertheless, the equilibrium  $\beta$  limit has not been reached, so far. In the upper part of Fig. 4 the surfaces of constant soft X-ray emission intensity are shown as are obtained by tomographic reconstruction using 2 soft X-ray cameras [8]. They are in good agreement with the NEMEC results. Though in high  $\beta$  configurations with  $\beta_0 = 4\%$  the magnetic well is reduced and NEMEC predicts resistive interchange unstable regions at the plasma edge no instabilities have been observed, so far.

### 3.4 First steps to an island divertor

The W7-AS "high iota" configurations ( $\text{iota} > 0.5$ ), bounded by "natural" islands of considerable size, have the basic edge topology required for an island divertor. The presently installed target arrangement (10 inboard target plates, preserving both the fivefold periodicity and up/down symmetry of the configuration) is the first step on the way to an optimised divertor, which will start operation within the next two years.

Extensive measurements of the island edge structures by plasma spectroscopy and target calorimetry are in excellent agreement with predicted vacuum and equilibrium configurations, which are available up to central  $\beta$  values of  $\approx 1\%$ . Analysis of high density NBI discharges for  $\iota = 5/9$  gives strong indications of stable high recycling conditions for  $\langle n_e \rangle \geq 10^{20} \text{ m}^{-3}$  [31]. The observations are reproduced by the 3D plasma edge transport code EMC3 [32] which has been coupled selfconsistently to the EIRENE [34] neutral gas code.

For low density ECRH discharges, poloidal asymmetries in the island SOL have been observed for  $\iota = 5/9$  configurations, with the islands deeply cut by the inboard plates through the O-point (Fig. 5(a)) [33]. Higher densities from Langmuir probe array data were measured for the lower or upper island fans, depending on the  $B$  field direction (Fig. 5(b)). The asymmetries can be explained by the effects of an  $E_r \times B$  drift driven by the radial temperature gradient in the island which leads to a radial gradient of the electrostatic potential. The poloidal density gradient also implies an

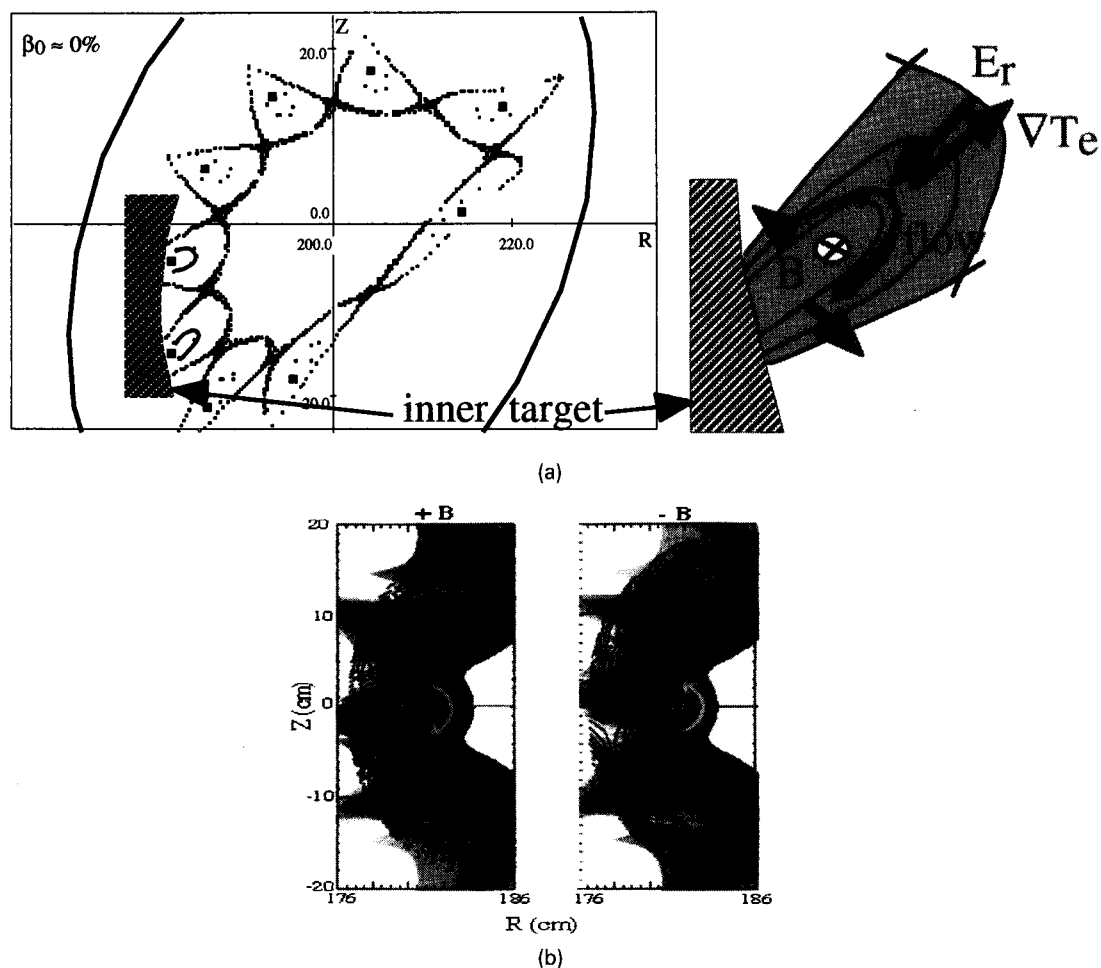


Fig. 5 (a) left: Poloidal cross section of the  $\tau = 5/9$  configuration at the poloidal plane of an inboard plate, right: Flow to target plate resulting from the  $E_r \times B$  drift (schematic).  
 (b) Density contour from probe array (curves) compared to EMC3/EIRENE results for positive and negative B-field. For positive (negative) B the deposition maximum is shifted downward (upward).

imbalance of the power and particle fluxes to the plates, which is consistent with calorimetric and  $H_\alpha$  measurements. The drift velocities resulting from estimated radial temperature gradients were inserted into the EMC3/EIRENE code, leading to the same phase shift of the density contours as experimentally observed (Fig. 5(b)).

### 3.5 Heating scenarios with relevance for W7-X

The operation of W7-AS using ECR waves for heating (pure or in combination with NBI) as well as for start up of the plasma desires a proper adjustment of the magnetic field to meet the resonance condition:  $B_0 = 2.5$  T for 70 GHz fundamental O-mode and 140 GHz second harmonic X-mode and  $B_0 = 1.25$  T for 70 GHz second harmonic X-mode waves. Furthermore

ECRH is restricted in density because of the cut-off condition. Non resonant plasma build-up has been successfully carried out with turbulent Rf heating at a frequency of 900 MHz in combination with NBI at various magnetic fields between 0.6 and 2.5T (thus "non resonant") starting from a thin cold plasma ( $n_e < 10^{18} \text{ m}^{-3}$ ,  $T_e < 100$  eV). Another scenario which is neither restricted to a certain fixed magnetic field nor by an upper limit of the density is heating by electron Bernstein waves, EBW. Since these waves cannot be excited from outside the plasma they have to be generated by mode conversion from electromagnetic waves, e.g. in a so called O-X-B process. An O-mode wave launched with an optimum angle oblique to the magnetic field vector is converted into an X-mode at the O-mode cut-off density. This X-wave propagates towards the upper

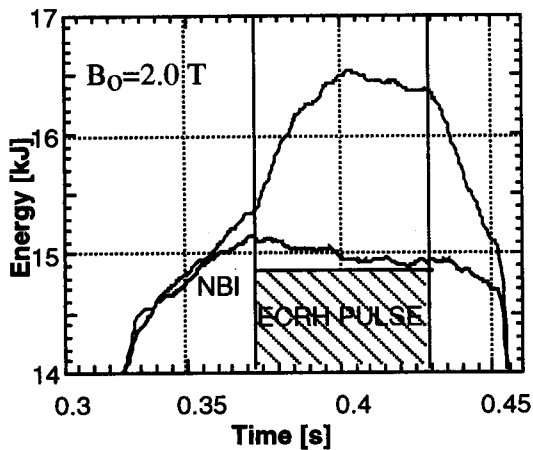


Fig. 6 Comparison of energy contents of a discharge heated by combined NBI and O-X-B (heating scenario with conversion from O-mode to X-mode to electron Bernstein waves) (upper curve) compared to a purely NBI heated one (lower curve) at  $B_0 = 2.0$  T with  $P_{\text{ECH}} = 220$  kW at 70 GHz and  $P_{\text{NBI}} \approx 720$  kW at a density of  $n_e(0) = 1.6 \times 10^{20} \text{ m}^{-3}$ .

hybrid resonance layer where it is converted into an EBW. This heating scenario has been successfully applied to W7-AS [14,15]. Figure 6 shows an example where at a non resonant magnetic field of  $B_0 = 2.0$  T an additional ECH pulse of  $P_{\text{ECH}} = 220$  kW has been applied to a NBI heated plasma with  $P_{\text{NBI}} \approx 720$  kW at a density of  $n_e(0) = 1.6 \times 10^{20} \text{ m}^{-3}$  which is well above the 70 GHz cut off density of  $n_e = 0.6 \times 10^{20} \text{ m}^{-3}$ . The O-X-B heating leads to a clear increase of the plasma energy content compared to the purely NBI heated case. Increases in the energy content up to 30% or 2.5 kJ ( $T_e^{\text{NBI}} \approx 360$  eV,  $\Delta T_e^{\text{OXB}} = 110$  eV) with  $P_{\text{ECH}} = 330$  kW and  $P_{\text{NBI}} \approx 360$  kW have been achieved, so far.

Long pulse operation in W7-X will need long pulse heating systems. Besides ECRH in cw operation ion cyclotron resonance heating, ICRH, is foreseen. Since matching of the outer magnetic surfaces with appropriate antenna systems turned out to be much more difficult for stellarators than for tokamaks, ICRH in stellarators is still in an experimental status. Nevertheless ICRH has been successfully operated at W7-AS for a pulse length up to 1 s [16]. Feeding 500 kW to a "broad antenna" [35] led to a deposition of about 200 kW into the plasma which had been built up by ECRH and taken over by ICRH via minority heating of hydrogen in a deuterium bulk plasma. The purely ICR heated plasma could be sustained up to 1 second. The electron temperature after dropping from about 2.5 keV during the phase of combined ECR and ICR heat-

ing to about 400 eV some time after the beginning of the purely ICR heated phase recovers to about 800 eV at the end of the ICRH pulse whereas the line integrated electron density remained constant at about  $0.16 \times 10^{20} \text{ m}^{-3}$ . During the whole ICRH pulse the impurity radiation remained low. In order to increase the power deposited in the plasma a double strap antenna will be installed during the next experimental campaign.

## References

- [1] U. Brossmann *et al.*, Nuclear Fusion, Suppl. (*Proc. 9th Int. Conf. on Plasma Phys. and Control. Nucl. Fusion Res.*, Baltimore, 1982), 141 (1983).
- [2] H. Renner *et al.*, Plasma Phys. Control. Fusion **31**, 1579 (1989).
- [3] A. Weller *et al.*, Plasma Phys. Control. Fusion **33**, 1559 (1991).
- [4] R. Brakel *et al.*, Plasma Physics and Control. Fusion, Suppl., *Proc. 24th EPS Conf. on Controlled Fusion and Plasma Physics*, (1997); Berchtesgaden, to be published.
- [5] H. Maassberg *et al.*, *Proc. 24th EPS Conf. on Controlled Fusion and Plasma Physics*, Berchtesgaden, Vol. IV, p.1605 (1997).
- [6] J. Baldzuhn *et al.*, in these Proceedings, p.226 (1998).
- [7] M. Kick *et al.*, *Proc. 10th International Stellarator Conference*, Madrid, p.330 (1995).
- [8] R. Jaenicke *et al.*, Plasma Phys. Control. Fusion **37**, A163 (1995).
- [9] M. Kick *et al.*, Fusion Energy (*Proc. of 16th IAEA Conf.*, Montréal 1996), F1-CN-64/C1-4, p.27 (1996).
- [10] U. Stroth *et al.*, *Proc. 24th EPS Conf. on Controlled Fusion and Plasma Physics*, Berchtesgaden, Vol. IV, p.1597 (1997).
- [11] V. Erckmann *et al.*, Plasma Phys. Control. Fusion **34**, 1917 (1992).
- [12] V. Erckmann *et al.*, 1997 Fusion Energy (*Proc. 16th IAEA Conf.*, Montréal, 1996), F1-CN-64/CP-1, p.119 (1996).
- [13] V. Erckmann *et al.*, Plasma Phys. and Control. Nucl. Fusion Res. (*Proc. 14th IAEA Conf. Würzburg, 1992*), Vol. II, IAEA-CN-56/C-1-8, p.469 (1992).
- [14] H. Laqua *et al.*, Phys. Rev. Lett. **78**, 3467 (1997).
- [15] H. Laqua *et al.*, in these Proceedings, p.314 (1998).
- [16] D.A. Hartmann *et al.*, *Proc. 24th EPS Conf. on Controlled Fusion and Plasma Physics*, Berchtesgaden, Vol. IV, p.1633 (1997).

- [17] N. Rust. *et al.*, *Proc. 24th EPS Conf. on Controlled Fusion and Plasma Physics*, Berchtesgaden, Vol. IV, p.1621 (1997).
- [18] H. Maassberg *et al.*, in these Proceedings, p.103 (1998).
- [19] S. Murakami *et al.*, in these Proceedings, p.122 (1998).
- [20] P. Grigull *et al.*, in these Proceedings, p.291 (1998).
- [21] M. Anton *et al.*, in these Proceedings, p.259 (1998).
- [22] A. Weller *et al.*, *Proc. 24th EPS Conf. on Controlled Fusion and Plasma Physics*, Berchtesgaden, Vol. IV, p.1649 (1997).
- [23] A. Weller *et al.*, *Phys. Rev. Lett.* **72**, 1220 (1994).
- [24] S.P. Hirshman *et al.*, *Phys. Fluids* **29**, 2951 (1986); W.I. Van Rij, S.P. Hirshman, *Phys. Fluids* **B1** 563 (1989).
- [25] H. Maassberg *et al.*, *Phys. Fluids* **B5**, 3627 (1993).
- [26] U. Stroth *et al.*, *Nucl. Fusion* **36**, 1063 (1996).
- [27] J. Baldzuhn, W. Ohlendorf and W7-AS Team, *Rev. Scient. Instrum.* **68** (1), 1020 (1997).
- [28] P. Grigull, *private communication*.
- [29] C. Beidler, J. Geiger, J. Kisslinger and H. Maassberg, *Proc. 10th International Stellarator Conference*, Madrid, p.326 (1995).
- [30] S.P. Hirshman *et al.*, *Comput. Phys. Comm.* **43**, 143 (1986).
- [31] F. Sardei *et al.*, *J. Nucl. Mater.* **241-243**, 135 (1997).
- [32] Y. Feng *et al.*, *J. Nucl. Mater.* **241-243**, 930 (1997).
- [33] Y. Feng *et al.*, *Proc. 24th EPS Conf. on Controlled Fusion and Plasma Physics*, Berchtesgaden, Vol. IV, p.1569 (1997).
- [34] D. Reiter, The GRENE code, KFA Jülich Report, Jül-1947 (1985).
- [35] G. Cattanei *et al.*, *Nucl. Fusion* **29**, 15 (1989).